ACS APPLIED MATERIALS & INTERFACES

Research Article

www.acsami.org

Improved Power Conversion Efficiency of Inverted Organic Solar Cells by Incorporating Au Nanorods into Active Layer

Yeyuan He,[†] Chunyu Liu,[†] Jinfeng Li,[†] Xinyuan Zhang,[†] Zhiqi Li,[†] Liang Shen,[†,‡] Wenbin Guo,*[,†] and Shengping Ruan[†]

[†]State Key Laboratory on Integrated Optoelectronics, Jilin University, 2699 Qianjin Street, Changchun 130012, People's Republic of China

[‡]Department of Mechanical and Materials Engineering and Nebraska Center for Materials and Nanoscience, University of Nebraska−Lincoln, Lincoln, Nebraska 68588-0656, United States

ABSTRACT: This Research Article describes a cooperative plasmonic effect on improving the performance of organic solar cells. When Au nanorods (NRs) are incorporated into the active layers, the designed project shows superior enhanced light absorption behavior comparing with control devices, which leads to the realization of organic solar cell with power conversion efficiency of 6.83%, accounting for 18.9% improvement. Further investigations unravel the influence of plasmonic nanostructures on light trapping, exciton generation, dissociation, and charge recombination and transport inside the thin films devices. Moreover, the introduction of high-conductivity Au NRs improves electrical conductivity of the whole device, which contributes to the enhanced fill factor.

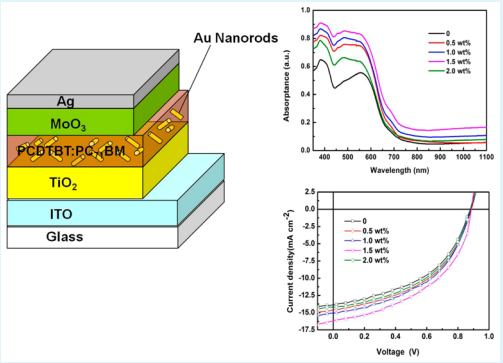

KEYWORDS: *organic solar cells, Au nanorods, plasmonic effect, scattering effect, exciton generation, charge transport*

1. INTRODUCTION

Predictions associated with limited fossil fuels and environmental issues caused by them have motivated a rapid growth of research on photovoltaics (PVs). Up to now, the majority of PVs are silicon-based conventional P−N junction devices, however, the dominance of these PVs is being challenged by the emergence of so-called organic solar cells (OSCs) based on new materials and device approaches.[1] OSCs technologies based on solution processing methods show a series of advantages that conventional silicon-based devices do not have, such as, low cost, ease of fabrication, flexibility, and lightweight.[2−5] In spite of these virtues, OSCs are still far away from commercial application because of their low power conversion efficiency (PCE). The overall PCE of OSC devices is highly dependent on the thickness of the active layer film.[6−8] On one hand, light absorption and subsequent exciton generation, are directly proportional to the film thickness. That is to say, a thicker film has a higher absorption and increases the number of potential charge carriers through the increase of photoactive material. However, on the other hand, a thinner active layer lowers the probability of excition recombination and thus increases the excition collection efficiency. Obviously, developing approaches to increase effective light trapping in the active film which is as thin as possible is the key challenge in improving device efficiency.

Recently, metallic nanopaticles (NPs) were introduced into organic photovoltaic (OPV) devices for highly improved light harvesting by utilizing the localized surface plasmonic resonances (LSPR) effects,[9−15] scattering effects,[16−18] and the synergy of both.[19−22] The field of NPs plasmonics has been widely studied during the last two decades, leading to the discovery of some very interesting phenomenon and the development of applications in photoelectric conversion.[23−25] The electric field component of incident electromagnetic radiation can excite the sea of conduction band electrons associated with the metal particle at a resonant mode which causes the electrons to oscillate coherently on the surface of the particle. This phenomenon is referred to as LSPR.[26] However, the influence of NPs on charge separation and transport inside high efficiency solar cells still needs to be deeply explored.[27]

In this work, we report a cooperative PCE enhancement of 18.9% by simply introducing Au nanorods (NRs) into active layers of OSCs fabricated from Poly [N-900-hepta-decanyl-2,7-carbazolealt-5,5-(40,70-di-2-thienyl-20,10,30-benzothiadiazole)(PCDTBT) and [6,6]-phenyl C_{71}-butyric acid methyl ester ($PC_{71}BM$). It is demonstrated here that incorporation of NRs exhibits distinct advantages of light harvesting enhancement and charge transport properties improvement.

Received: April 9, 2015
Accepted: July 7, 2015
Published: July 7, 2015

DOI: 10.1021/acsami.5b03024
ACS Appl. Mater. Interfaces 2015, 7, 15848−15854

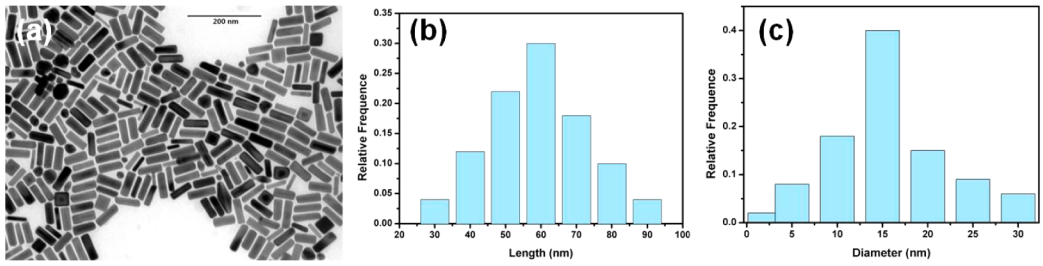

Figure 1. (a) TEM images of Au NRs. (b) Histogram of Au NRs length. (c) Histogram of Au NRs diameter.

2. EXPERIMENTAL SECTION

2.1. Preparation of Active Layer Solution. For the synthesis of Au NRs, 1 mL of 1 wt % chloroauric acid ($HAuCl_4$) was dissolved in 99 mL of deionized water and refluxed, following with 1 wt % sodium citrate solution adding to the boiling solution under stirring. The Au NRs solution formed after further boiling for 30 min and cooling to room temperature. The synthesized Au NRs were dissolved in tetrahydrofuran (THF, 99.99%) eventually. For the preparation process of the active layer solution, Au solution was first added into a bottle, subsequently dried with nitrogen. At the preparation process of the active layer solution, Au solution was first added into a bottle, subsequently dried with nitrogen. Then PCDTBT, $PC_{71}BM$, and 1,2-dichlorobenzene (DCB) solution were added successively. Thus, we got five kinds of active layer solution containing various weight ratio (wt) (0, 0.5, 1.0, 1.5, and 2.0 wt %) of Au NRs. The active layer solutions were sealed and stirred for 72 h in air without illumination. The active layers were annealed in glovebox after spin-casting in glass substrate. All measurements of device performance were done in air. Figure 1 shows the transmission electron microscope (TEM) image (Figure 1a), length histogram (Figure 1b), and diameter histogram (Figure 1c) of synthesized Au NRs. It can be seen that the NRs are 60 nm in length and 15 nm in diameter on average, which are comparable to the thickness of the active layer (100 nm). The film thickness was tested by Spectroscopic Ellipsometry (SE). Therefore, it is safe to assume that NRs are embedded within active layer and LSPR are induced in solar cells.

2.2. Device Fabrication and Characterization. OSC devices containing different concentration of Au NRs in active layer film were fabricated with the structure of indium tin oxide (ITO)/titanium dioxide (TiO_2)/PCDTBT: $PC_{71}BM$/molybdenum oxide (MoO_3)/sliver (Ag) on clean ITO/glass substrates, which is shown in Figure 2.

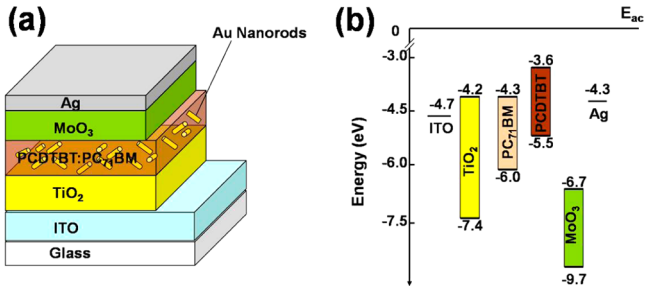

Figure 2. (a) Device structure of the inverted OSCs. (b) Scheme of energy levels of devices based on PCDTBT: $PC_{71}BM$.

The patterned ITO/glass substrates were cleaned with acetone, ethanol, and deionized water in order under ultrasonic processing for 20 min, respectively. Then colloid TiO_2 prepared by sol−gel method was spin-cast at 3000 rpm (rpm) onto the substrates and annealed at 450∘C for 2 h, acting as electron transport layer of OSC. For the active layer, PCDTBT:$PC_{71}BM$ solution with varying concentration of Au NRs was subsequently spin-cast on the top of TiO_2 layer at 2000 rpm and annealed at 70∘C for 10 min in the atmosphere of argon. MoO_3 acting as hole transport layer does good to hole collection at the photoactive layer interface,[28−31] which was deposited onto the active film layer through thermal evaporation with a thickness of 4 nm. In the end, the devices were finished with 100 nm Ag deposited as anode. Single-carrier devices with the structure of ITO/TiO_2/PCDTBT: $PC_{71}BM$/BCP/Ag or ITO/MoO_3/PCDTBT: $PC_{71}BM$/MoO_3/Ag were also fabricated using the same method. For the device characterizations, Transmission electronic modules (TEM) measurement, $J-V$ characteristics of normal devices, and single-carrier devices, atomic force microscope (AFM) measurement, absorption and transmission spectra, incident photon-to-current efficiency (IPCE), and impedance spectroscopy were carried out as described in our published papers.[32,33]

3. RESULTS AND DISCUSSION

Figure 3 illustrates AFM images of active layer without and with 1.5 wt % NRs doping. The root-mean-squared (RMS) roughness of pristine PCDTBT: $PC_{71}BM$ film (Figure 3a) is measured to be 1.51 nm while active layer mixed with 1.5 wt % NRs exhibits exactly the same RMS roughness (Figure 3b). So we could anticipate that all the NRs were located within active layer thus the RMS roughness remains unchanged. In addition, the active layer with 1.5 wt % Au NRs surface presents an obvious and homogeneous phase separation (Figure 3c), which cannot be observed from the active layer without Au NRs

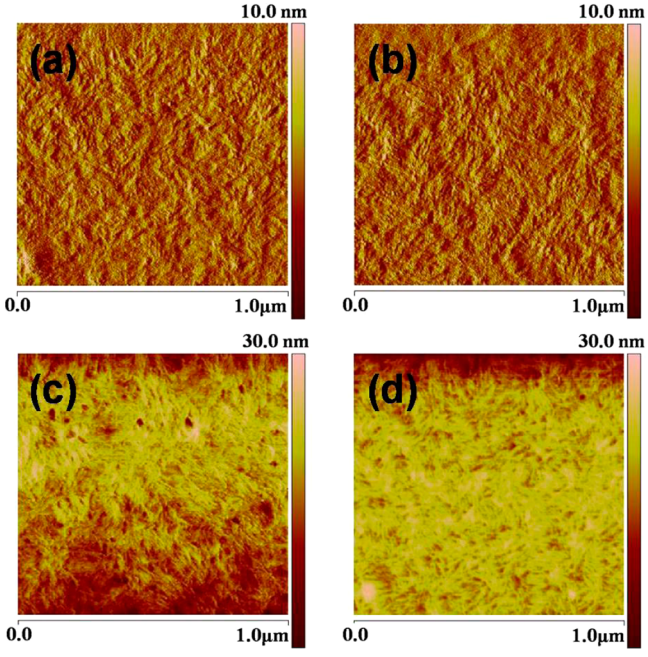

Figure 3. AFM images of active layer films,(a) height image of pristine PCDTBT:$PC_{71}BM$ film, (b) height image of PCDTBT:$PC_{71}BM$ film with 1.5 wt % NRs doping, (c) phase image of PCDTBT:$PC_{71}BM$ film with 1.5 wt % NRs doping, and (d) phase image of pristine PCDTBT:$PC_{71}BM$ film.

DOI: 10.1021/acsami.5b03024
ACS Appl. Mater. Interfaces 2015, 7, 15848−15854

(Figure 3d). The doped films show uniformly percolated structures and flat surfaces.[34] It is well recognized that continuous interpenetrating networks with proper domain size play an important role in exciton separation and charge transport.[35,36]

The current density−voltage (J−V) curves of photoactive devices containing various concentrations of Au NRs are presented in Figure 4, with the performance details summarized

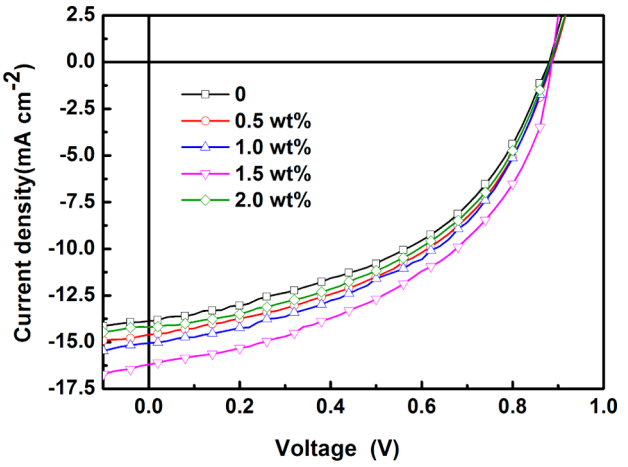

Figure 4. J−V curves of OSCs without and with various concentrations of Au NRs doping.

in Table 1, and all the values are typically average of 50 devices. The cells were measured with a shadow mask and only ITO-coated glass was exposed to light. Actually, all the devices we fabricated were optimized aiming at getting maximum PCE. The optimized control device without Au NRs shows a PCE of 5.74%, corresponding open-circuit voltage (V_{oc}) of 0.88 V, short-circuit current density (J_{sc}) of 13.87 mA/cm^2, fill factor (FF) of 47.0%. When Au NRs was blended, as anticipated, J_{sc} and FF increase gradually with the concentration of blending Au NRs from 0.5 wt % to 1.5 wt % with unchanged V_{oc}. However, when the doping concentration continually increases to 2.0 wt %, J_{sc} and FF begin to decrease and result in of PCE of only 5.94%. The optimum concentration of 1.5 wt % Au NRs provides the best device performance, J_{sc} of 16.10 mA/cm^2, V_{oc} of 0.88 V and FF of 48.1%, leading to a PCE of 6.83% and 18.9% higher than control device. Notably, the lager FF of doping devices can be put down to the increased charge mobility and reduced resistance (R_s).[34,37−39] IPCE measurements of five different solar cells are conducted to better elucidate improved J_{sc}, and the J_{sc} calculated from IPCE curves were also shown in Table 1. Figure 5 depicts the corresponding IPCE spectra (Figure 5a) and IPCE difference of doped and control device. For the doping solar cells, IPCE exhibits significant increase covering a broad wavelength range from 400 to 700 nm compared to the control device, corresponding

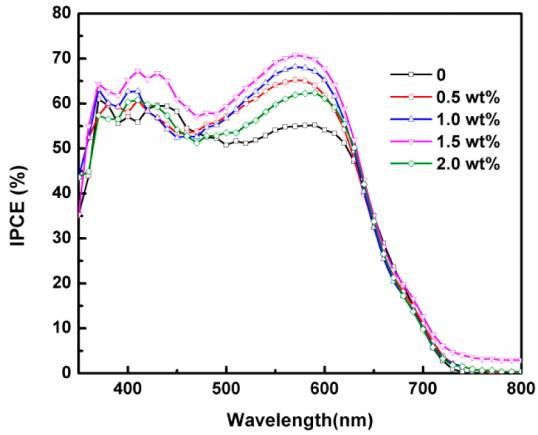

Figure 5. IPCE characteristic of OSCs without and with various concentrations of Au NRs doping.

to the J-V characteristics presented in Figure 4, and this indicates direct evidence for the enhanced J_{sc}. The measured J_{sc} from the OSC devices were well-matched with the J_{sc} calculated from integration of IPCE curves (within 10% error), which confirmed the accuracy of PCE from the measurement.

To better illustrate the J_{sc} enhancement, we did a simulation of electric field profiles of active layer with Au NRs using finite-difference time-domain (FDTD) methods (FDTD SOLUTIONs from Lumerical Solutions, Inc.). The blend PCDTBT:PC$_{71}$BM was treated as a single effective medium in our simulation. The optical field was calculated with Au NRs distributing in active layer. The values of Au NRs were got from the histogram of both dimensions. The absorption and extinction coefficients of PCDTBT:PC$_{71}$BM blend film were measured by SE, and the refractive index of the film was measured from 300 to 1100 nm, which included absorption and extinction coefficient. The optical field simulation was implemented via Au NRs embedding in blend film. The theoretical analog results of electric field profiles in Au NRs doped active layers in the wavelength of 532 (Figure 6a) and

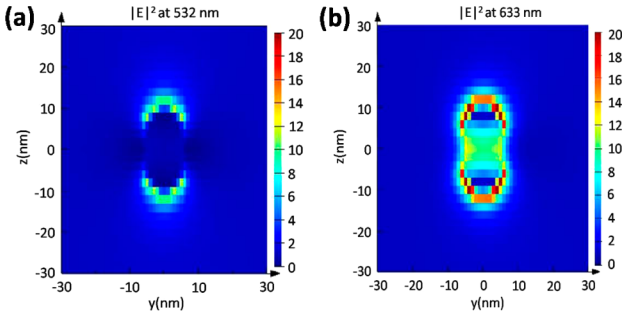

Figure 6. LSPR effect simulation for active layer doping with Au NRs at the wavelength of (a) 532 and (b) 633 nm.

Table 1. Detail Performance Parameters of All d OSC Devices without or with Different Ratios Au Nanorods Doping

Au NRs (wt %)	V_{oc} (V)	J_{sc} (mA cm^{-2})	J_{sc} of IPCE (mA cm^{-2})	FF (%)	PCE (%)	R_s (Ω)	R_{sh} (Ω)
0	0.88	13.87 ± 0.01	11.93	47.0	5.74 ± 0.11	236.02	3125.35
0.5	0.88	14.60 ± 0.01	12.87	47.7	6.12 ± 0.08	221.25	5680.24
1.0	0.88	15.06 ± 0.04	13.16	47.8	6.44 ± 0.13	195.04	6839.59
1.5	0.88	16.10 ± 0.03	14.05	48.1	6.83 ± 0.05	171.95	9852.81
2.0	0.88	14.19 ± 0.02	12.28	47.6	5.94 ± 0.12	229.06	5006.29

DOI: 10.1021/acsami.5b03024
ACS Appl. Mater. Interfaces 2015, 7, 15848−15854

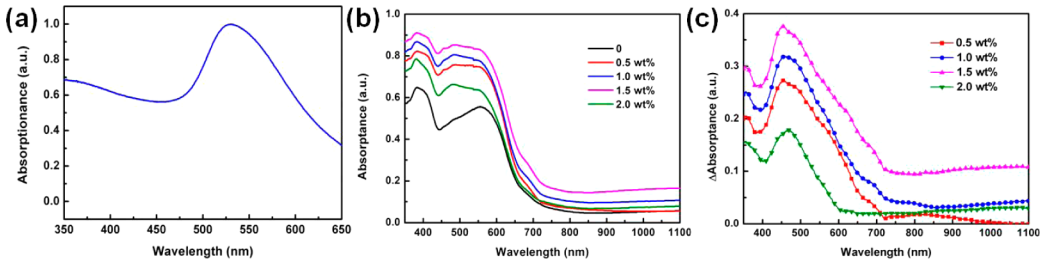

Figure 7. (a) Absorption spectrum of Au NRs, (b) absorption spectra of PCDTBT: $PC_{71}BM$ film doped with various concentrations of Au NRs, and (c) absorption difference of doped active layer films and undoped films.

633 nm (Figure 6b) are shown in Figure 6. The color scale corresponds with the magnitude of increased electric field intensity. This indicates that resonant near-field enhancement is the primary mechanism contributing to enhanced absorption with a small addition contribution from enhanced far-field scattering into the optical modes of the device. The absorption gain results in J_{sc} enhancement.[40] It has been announced that Au and Ag nanoparticles can play as an effective antenna for the incident light that stores photon energy in a localized surface plasmon mode.[41,42] Some effects may also exist, such as scattering effect, enlargement of the effective medium dielectric constant (high-*k* materials), and local increase of the degree of spin−orbit coupling for allowing intersystem crossing (ISE).

We also performed UV−vis absorption spectra of Au NRs (Figure 7a), whose peak locates in 550 nm. The absorption spectrum of PCDTBT: $PC_{71}BM$ blended films with various concentrations of Au NRs is shown in Figure 7b, which was directly spin-cast on clean glass at 2000 rpm and annealed at 70 °C for 10 min in the atmosphere of argon. The absorption difference of doped films and pristine active layer is shown in Figure 7c. Obviously, once Au NRs were doped, the blended film shows greater optical absorption covering the wavelength range from 350 to 700 nm. Partly, we attribute the enhanced optical absorption to LSPR and scattering effect of Au NRs. In addition, Au NRs can reflect and scatter light and therefore increase the optical path length within the active film. The thin film thickness of active layer was got by SE, which varied a little under a small amount of Au NRs doping. Therefore, light trapping enhancement in doped films did not result from thickness increase, which really originated from doping effect. On the basis of IPCE and UV−vis absorption results, it is clear that NRs doping greatly broaden the wavelength range for enhancement compared with pristine active layer. Thus, the introduction of Au NRs to active film offers the possibility of enhanced optical absorption and correspondingly enhanced photoinduced carriers.[43−46]

The photoluminescence (PL) is measured to further examine the exciton dissociation in the active layer films. Figure 8 shows the PL spectra of the pristine PCDTBT:$PC_{71}BM$ film and active layer films with different weight ratio of Au NRs annealed at 70 °C for 10 min. The PL signals are corrected with the absorption spectra of the active layers with different weight ratio at wavelength of 450 nm. PL quenching is observed for the active layer film with 0.5, 1.0, and 1.5 wt % Au NRs comparing to that without Au NRs. This provides a direct evidence for enhanced exciton dissociation and reduced electron/hole recombination by incorporating the NRs, which can also make contribution to the performance improvement of OSCs.

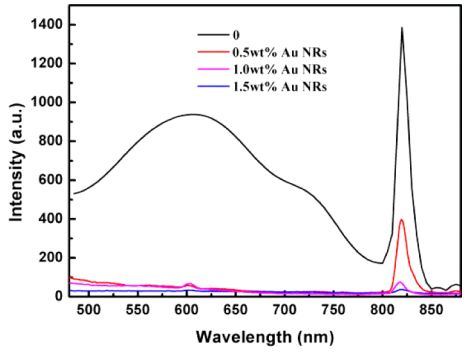

Figure 8. Photoluminescence spectra of active layers with various concentrations of Au NRs.

Simultaneously with the drastic enhancement in J_{sc}, the FF of the optimized devices is found to improve moderately, suggesting that the charge transport properties are improved. To make a realistic evaluation on the charge carrier mobility in the active layer, electron-only and hole-only devices were both fabricated, and $J-V$ characteristics were measured and fitted using the space-charge-limited current (SCLC) model (Figure 9). The corresponding device structures are also inserted in Figure 9a and b. For the electron-only devices (Figure 9a), those doping with various concentrations of Au NRs indicate larger current density in contrast to the control device, and the maximum current emerges at the concentration of 1.5 wt %, conforming to Figure 4. For the hole-only devices (Figure 9b), the result is similar. To explain the better charge transfer properties, the hole and electron mobilities were calculated using SCLC model. Hole mobility increases from 1.9×10^{-4} to 2.2×10^{-3} cm^2 V^{-1} s^{-1}, and electron mobility increases from 2.1×10^{-4} to 2.3×10^{-3} cm^2 V^{-1} s^{-1}. Upon the incorporation of Au NRs, both the electron and hole mobilities increase, leading to a dramatic enhancement of charge collection efficiency for both electrodes.

To further investigate the effect of Au NRs on the optical absorption of OSCs, the photocurrent density (J_{ph})−effective voltage (V_{eff}) curve was made and shown in Figure 10a. J_{ph} is defined as $J_{ph} = J_L - J_D$, in which J_L and J_D stand for the current density of OSC device under illumination and in the dark, respectively. V_{eff} is defined as $V_{eff} = V_0 - V$, in which V_0 is the voltage where $J_{ph} = 0$ and V is the applied bias voltage. As is shown in Figure 10a, J_{ph} tends to saturate at high V_{eff} after increasing linearly at low V_{eff} range, and thus we get the definition of saturation photocurrent density (J_{sat}) which assumes that all the photogenerated excitons are dissociated into free charge carriers and collected by electrodes afterward under high V_{eff}.[35,36] Then we determine the maximum exciton generation rate (G_{max}) from the equation $J_{sat} = qG_{max}L$, where q

DOI: 10.1021/acsami.5b03024
ACS Appl. Mater. Interfaces 2015, 7, 15848−15854

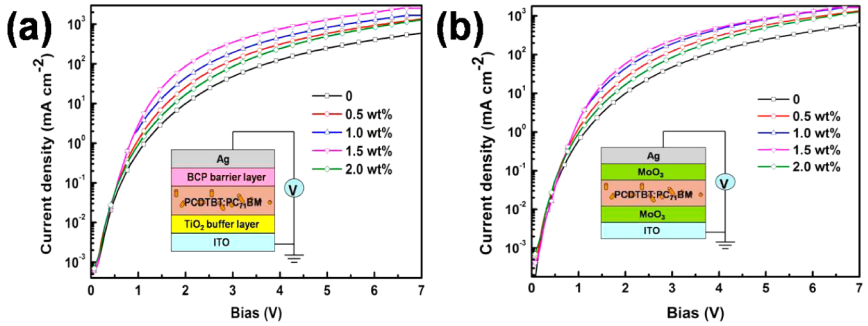

Figure 9. $J-V$ characteristics of the single-carrier devices, (a) single-electron device, (b) single-hole device, and (inset) the structure of the single-carrier devices.

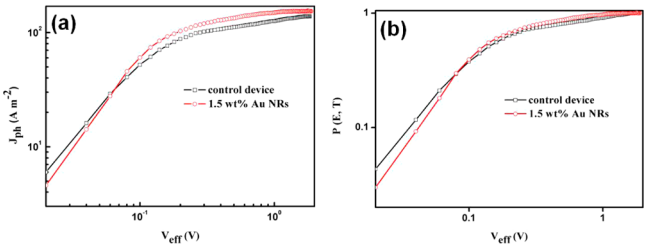

Figure 10. (a) Photocurrent density (J_{ph}) as a function of the effective voltage (V_{eff}) for control and doped devices under constant incident light intensity and (b) exciton dissociation probability [$P(E,T)$] plotted with respect to effective bias (V_{eff}) for these OSC devices.

is the electronic charge and L is the thickness of active layer (100 nm). Therefore, we get the values of G_{max} for the control and doped devices: 8.62×10^{27} (J_{sat} = 138 A m^{-2}) and 9.56×10^{27} m^{-3} s^{-1} (J_{sat}= 153 A m^{-2}), respectively. Obviously, an noticeable enhancement of G_{max} is obtained by incorporating Au NRs into the active layer. Thus, we can come to the conclusion that the light absorption in the active layer of doped devices increases remarkably, since G_{max} is related to maximum absorption of incident photons. So the Au NRs demonstrate a positive effect on the light absorption and contribute to generation of the photogenerated excitons. The exciton dissociation probabilities[$P(E,T)$], which are related to the electric field (E) and temperature (T), are important signs of exciton dissociation level. In the active layer, only a part of photogenerated excitions can be dissociated into free carriers, and as a result, J_{ph} can be determined as $J_{ph} = qG_{max}P(E,T)L$. Thus, the value of $P(E,T)$ at any bias can be obtained from the equation $P(E, T) = J_{ph}/J_{sat}$. Figure 10b shows that the value of $P(E,T)$ under the short-circuit conditions (V_a = 0 V) increases from 90.8% for the reference device to 96.6% for the doped device, indicating that excitation of the LSPR also facilitated excitons to dissociate into free carriers. In conclusion, incorporation of Au NRs in active layer increase both the exciton generation rate and the dissociation probability, thereby enhancing(enhances) the photocurrent of the OSCs.

Impedance spectroscopy has been successfully applied in the field of inorganic solar cells and OSCs to obtain valuable information about kinetics and energetic processes that govern the device performance.[47] Also, it is an essential tool to observe bulk and electrical properties that cannot be observed in direct current regime.[48] In the literature, different equivalent circuit models have been proposed to simulate the impedance of OSCs. Here we use the simple parallel RC model to observe the interfacial electrical properties of fabricated devices, with the results shown in Figure 11. The measurement was done under the frequency of 20 to 1 MHz. In the simple parallel RC

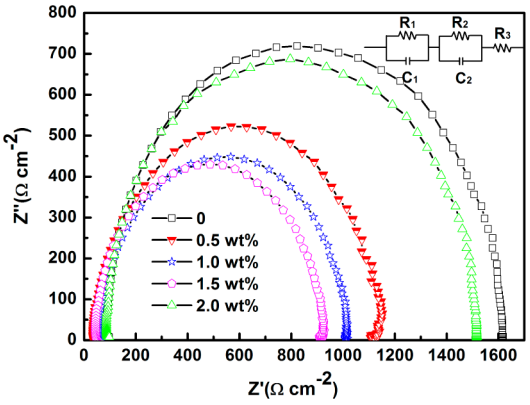

Figure 11. Impedance spectra diagram of the finished devices, inset graph is the equivalent circuit model of solar cells.

model, the impedance spectra are in the shape of semicircle, and the larger semicircle means larger impedance. Apparently, the devices with Au NRs have much smaller impedance, which indicates that the incorporation of Au NRs brings about significant improvement of interfacial electrical property and the resultant enhanced J_{sc}. Series resistance (R_s) and shunt resistance (R_{sh}) were also estimated and listed in Table 1. By comparing the records, we find that the control device has the largest R_s of 236.02 Ω and the smallest R_{sh} of 3125.35 Ω, and in contrast, the device doping 1.5 wt % Au NRs has the smallest R_s of 171.95 Ω and the largest R_s of 9852.81Ω. This coincides with Figures 4 and 5, and demonstrates the effect of Au NRs on J_{sc}.

As we know, the structural characteristics are well correlated to photovoltaic properties for organic solar cells.[49] The morphology of the active layer can be remarkably tuned by a certain amount of incorporated Au NRs. The specific NRs-containing phase can assist the aggregation of PC$_{71}$BM molecules into the clusters during phase separation of film formation. The network of the dispersed NRs forming an additional interpenetrating network provides a more efficient pathway for transport of charge carriers and thus significantly enhances the PCE value and photovoltaic properties. The Au NRs used in this study are expected to possess a work function of approximately 5.1 eV, which is close to the HOMO energy level of PCDTBT of 5.5 eV, thus resulting in a small energy barrier for hole extraction. As shown in Table 1, the use of Au NRs might lead to a reduced series resistance because the holes

DOI: 10.1021/acsami.5b03024
ACS Appl. Mater. Interfaces 2015, 7, 15848−15854

need to pass through fewer interfaces than in the pristine active layer.[34]

4. CONCLUSION

To conclude, we improved the PCEs of OSCs by incorporating Au NRs into active layer. LSPR-induced local field enhancement not only leads to increased light absorption of active layer materials but also benefits charge separation and transport, leading to enhanced J_{sc}, FF, and IPCE. These improvements result from enhanced optical absorption caused by the combination of LSPR and light scattering of Au NRs. Also, increased carrier mobility caused by high-conductivity Au NRs results in low R_s. For the optimized doping concentration of 1.5 wt % Au NRs, a high PCE of 6.83% was achieved by this way. We believe that our study offers an effective approach to enhance the efficiency of OSCs and may be shed light on the other research on solar cell devices.

AUTHOR INFORMATION

Corresponding Author

*E-mail: guowb@jlu.edu.cn.

Notes

The authors declare no competing financial interest.

ACKNOWLEDGMENTS

The authors are grateful to National Natural Science Foundation of China (61275035, 61370046), Chinese National Programs for High Technology Research and Development (2013AA030902), Project of Science and Technology Development Plan of Jilin Province (20120324, 20130206075SF), Scientific Frontier and Interdiscipline Innovative Projects of Jilin University (2013ZY18), Key Technology Research and Development Program of Changchun (13KG66), the Opened Fund of the State Key Laboratory on Integrated Optoelectronics (IOSKL2012KF03), and Project of Graduate Innovation Fund of Jilin University (2015098) for the support to the work.

REFERENCES

(1) Li, X. C.; Xie, F. X.; Zhang, S. Q.; Hou, J. H.; Choy, W. C. H. MoO_x and V_2O_x as Hole and Electron Transport Layers Through Functionalized Intercalation in Normal and Inverted Organic Optoelectronic Devices. *Light: Sci. Appl.* **2015**, *4*, e273.

(2) Nielsen, T. D.; Cruickshank, C.; Foged, S.; Thorsen, J.; Krebs, F. C. Business, Market and Intellectual Property Analysis of Polymer Solar Cells. *Sol. Energy Mater. Sol. Cells* **2010**, *94*, 1553−1571.

(3) Edwards, C.; Arbabi, A.; Popescu, G.; Goddard, L. L. Optically Monitoring and Controlling Nanoscale Topography During Semiconductor Etching. *Light: Sci. Appl.* **2012**, *1*, e30.

(4) Krebs, F. C.; Nielsen, T. D.; Fyenbo, J.; Wadstrøm, M.; Pedersen, M. S. Manufacture, Integration and Demonstration of Polymer Solar Cells in a Lamp for the "Lighting Africa" Initiative. *Energy Environ. Sci.* **2010**, *3*, 512−525.

(5) Brabec, C. J.; Gowrisanker, S.; Halls, J. J. M.; Laird, D.; Jia, S.; Williams, S. P. Polymer−Fullerene Bulk-Heterojunction Solar Cells. *Adv. Mater.* **2010**, *22*, 3839−3856.

(6) Boland, P.; Namkoong, G. Optimization of Active Layer Thickness in Planar Organic Solar Cells via Optical Simulation Methods. *Jpn. J. Appl. Phys.* **2010**, *49*, 030205.

(7) Hazar Apaydin, D.; Yildiz, D. E.; Cirpan, A.; Toppare, L. Optimizing the Organic Solar Cell Efficiency: Role of the Active Layer Thickness. *Sol. Energy Mater. Sol. Cells* **2013**, *113*, 100−105.

(8) Rahmani, R.; Karimi, H.; Ranjbari, L.; Emadi, M.; Seyedmahmoudian, M.; Shafiabady, A.; Ismail, R. Structure and Thickness Optimization of Active layer in Nanoscale Organic Solar Cells. *Plasmonics* **2015**, *10*, 495−502.

(9) Gan, Q.; Bartoli, F. J.; Kafafi, Z. H. Plasmonic-Enhanced Organic Photovoltaics: Breaking the 10% Efficiency Barrier. *Adv. Mater.* **2013**, *25*, 2385−2396.

(10) Ferry, V. E.; Munday, J. N.; Atwater, H. A. Design Considerations for Plasmonic Photovoltaics. *Adv. Mater.* **2010**, *22*, 4794−4808.

(11) Stratakis, E.; Kymakis, E. Nanoparticle-based Plasmonic Organic Photovoltaic Devices. *Mater. Today* **2013**, *16*, 133−146.

(12) Wang, C. C. D.; Choy, W. C. H.; Duan, C. H.; Fung, D. D. S.; Sha, W. E. I.; Xie, F. X.; Huang, F.; Cao, Y. Optical and Electrical Effects of Gold Nanoparticles in the Active Layer of Polymer Solar Cells. *J. Mater. Chem.* **2012**, *22*, 1206−1211.

(13) Li, X. H.; Choy, W. C. H.; Lu, H. F.; Wei, E. I.; Sha, W. E. I.; Ho, A. H. P. Efficiency Enhancement of Organic Solar Cells by Using Shape-Dependent Broadband Plasmonic Absorption in Metallic Nanoparticles. *Adv. Funct. Mater.* **2013**, *23*, 2728−2735.

(14) Spyropoulos, G. D.; Stylianakis, M. M.; Stratakis, E.; Kymakis, E. Organic Bulk Heterojunction Photovoltaic Devices with Surfactant-free Au Nanoparticles Embedded in the Active Layer. *Appl. Phys. Lett.* **2012**, *100*, 213904.

(15) Lu, L. Y.; Luo, Z. Q.; Xu, T.; Yu, L. P. Cooperative Plasmonic Effect of Ag and Au Nanoparticles on Enhancing Performance of Polymer Solar Cells. *Nano Lett.* **2013**, *13*, 59−64.

(16) Chen, L. Z.; Choy, W. C. H.; Wei, E. I.; Sha, W. E. I. Broadband Absorption Enhancement of Organic Solar Cells with Interstitial Lattice Patterned Metal Nanoparticles. *Appl. Phys. Lett.* **2013**, *102*, 251112.

(17) Baek, S. W.; Noh, J.; Lee, C. H.; Kim, B. S.; Seo, M. K.; Lee, J. Y. Plasmonic Forward Scattering Effect in Organic Solar Cells: A Powerful Optical Engineering Method. *Sci. Rep.* **2013**, *3*, 1726.

(18) Sha, W. E. I.; Choy, W. C. H.; Liu, Y. G.; Weng, C. C. Near-field Multiple Scattering Effects of Plasmonic Nanospheres Embedded into Thin-film Organic Solar Cells. *Appl. Phys. Lett.* **2011**, *99*, 113304.

(19) Kakavelakis, G.; Stratakis, E.; Kymakis, E. Aluminum Nanoparticles for Efficient and Stable Organic Photovoltaics. *RSC Adv.* **2013**, *3*, 16288−16291.

(20) Li, X. H.; Choy, W.C. H.; Huo, L. J.; Xie, F. X.; Sha, W. E. I.; Ding, B. F.; Guo, X.; Li, Y. F.; Hou, J. H.; You, J. B.; Yang, Y. Dual Plasmonic Nanostructures for High Performance Inverted Organic Solar Cells. *Adv. Mater.* **2012**, *24*, 3046−3052.

(21) Kakavelakis, G.; Stratakis, E.; Kymakis, E. Synergetic Plasmonic Effect of Al and Au Nanoparticles for Efficiency Enhancement of Air Processed Organic Photovoltaic Devices. *Chem. Commun.* **2014**, *50*, 5285−5287.

(22) González, D. M.; Körstgens, V.; Yao, Y.; Song, L.; Santoro, G.; Roth, S. V.; Müller-Buschbaum, P. Improved Power Conversion Efficiency of P3HT:PCBM Organic Solar Cells by Strong Spin-Orbit Coupling-Induced Delayed Fluorescence. *Adv. Energy Mater.* **2015**, *5*, 1401770.

(23) Atwater, H. A.; Polman, A. Plasmonics for Improved Photovoltaic Devices. *Nat. Mater.* **2010**, *9*, 205−213.

(24) Schuller, J. A.; Barnard, E. S.; Cai, W.; Jun, Y. C.; White, J. S.; Brongersma, M. L. Plasmonics for Extreme Light Concentration and Manipulation. *Nat. Mater.* **2010**, *9*, 193−204.

(25) Blum, O.; Shaked, N. T. Prediction of Photothermal Phase Signatures from Arbitrary Plasmonic Nanoparticles and Experimental Verification. *Light: Sci. Appl.* **2015**, *4*, e322.

(26) Wadams, R. C.; Yen, C.; Butcher, D. P., Jr.; Koerner, H.; Durstock, M. F.; Fabris, L.; Tabor, C. E. Gold Nanorod Enhanced Organic Photovoltaics: The Importance of Morphology Effects. *Org. Electron.* **2014**, *15*, 1448−1457.

(27) Lu, L. Y.; Luo, Z. Q.; Xu, T.; Yu, L. P. Cooperative Plasmonic Effect of Ag and Au Nanoparticles on Enhancing Performance of Polymer Solar Cells. *Nano Lett.* **2013**, *13*, 59−64.

(28) Meyer, J.; Hamwi, S.; Kroger, M.; Kowalsky, W.; Riedl, T.; Kahn, A. Transition Metal Oxides for Organic Electronics: Energetics, Device Physics and Applications. *Adv. Mater.* **2012**, *24*, 5408−5427.

DOI: 10.1021/acsami.5b03024
ACS Appl. Mater. Interfaces 2015, 7, 15848−15854

(29) Kroger, M.; Hamwi, S.; Meyer, J.; Riedl, T.; Kowalsky, W.; Kahn, A. P-type Doping of Organic Wide Band Gap Materials by Transition Metal Oxides: A Case-study on Molybdenum Trioxide. *Org. Electron.* **2009**, *10*, 932−938.
(30) Su, Y. H.; Ke, Y. F.; Cai, S. L.; Yao, Q. Y. Surface Plasmon Resonance of Layer-by-layer Gold Nanoparticles Induced Photoelectric Current in Environmentally-friendly Plasmon-sensitized Solar Cell. *Light: Sci. Appl.* **2012**, *1*, e14.
(31) Lepage, D.; Jimenez, A.; Beauvais, J.; Dubowski, J. J. Conic Hyperspectral Dispersion Mapping Applied to Semiconductor Plasmonics. *Light: Sci. Appl.* **2012**, *1*, e28.
(32) Li, X. H.; Choy, W.C. H.; Huo, L. J.; Xie, F. X.; Sha, W. E. I.; Ding, B. F.; Guo, X.; Li, Y. F.; Hou, J. H.; You, J. B.; Yang, Y. Dual Plasmonic Nanostructures for High Performance Inverted Organic Solar Cells. *Adv. Mater.* **2012**, *24*, 3046−3052.
(33) Li, L.; Li, T.; Tang, X. M.; Wang, S. M.; Wang, Q. J.; Zhu, S. N. Plasmonic Polarization Generator in Well-routed Beaming. *Light: Sci. Appl.* **2015**, *4*, e330.
(34) Wang, D. H.; Kim, J. K.; Seo, J. H.; Park, I. S.; Hong, B. H.; Park, J. H.; Heeger, A. J. Transferable Graphene Oxide by Stamping Nanotechnology: Electron-Transport Layer for Efficient Bulk-Heterojunction Solar Cells. *Angew. Chem., Int. Ed.* **2013**, *52*, 2874−2880.
(35) Park, B. C.; Yun, S. H.; Cho, C. Y.; Kim, Y. C.; Shin, J. C.; Jeon, H. G.; Huh, Y. H.; Hwang, I. C.; Baik, K. Y.; Lee, Y. I.; Uhm, H. S.; Cho, G. S.; Choi, E. H. Surface Plasmon Excitation in Semitransparent Inverted Polymer Photovoltaic Devices and Their Applications as Label-free Optical Sensors. *Light: Sci. Appl.* **2014**, *3*, e222.
(36) Zhu, Z. D.; Bai, B. F.; You, O. B.; Li, Q. Q.; Fan, S. S. Fano-resonance Boosted Cascaded Field Enhancement in a Plasmonic Nanoparticle-in-Cavity nanoantenna Array and Its SERS Application. *Light: Sci. Appl.* **2015**, *4*, e296.
(37) Fung, D. D. S.; Qiao, L. F.; Choy, W. C. H.; Wang, C. D.; Sha, W. E. I.; Xie, F. X.; He, S. L. Optical and Electrical Properties of Efficiency Enhanced Polymer Solar Cells with Au Nanoparticles in A PEDOT-PSS Layer. *J. Mater. Chem.* **2011**, *21*, 16349−16356.
(38) Kosten, E. D.; Atwater, J. H.; Parsons, J.; Polman, A.; Atwater, H. A. Highly Efficient GaAs Solar Cells by Limiting Light Emission Angle. *Light: Sci. Appl.* **2013**, *2*, e45.
(39) Wang, C. C. D.; Choy, W. C. H.; Duan, C.; Fung, D. D. S.; Sha, W. E. I.; Xie, F. X.; Huang, F.; Cao, Y. Optical and Electrical Effects of Gold Nanoparticles in the Active Layer of Polymer Solar Cells. *J. Mater. Chem.* **2012**, *22*, 1206−1211.
(40) Paz-Soldan, D.; Lee, A.; Thon, S. M.; Adachi, M. M.; Dong, H. P.; Maraghechi, P.; Yuan, M. J.; Labelle, A. J.; Hoogland, S.; Liu, K.; Kumacheva, E.; Sargent, E. H. Jointly Tuned Plasmonic-Excitonic Photovoltaics Using Nanoshells. *Nano Lett.* **2013**, *13*, 1502−1508.
(41) Su, Y.; Ke, Y.; Cai, S.; Yao, Q. Surface Plasmon Resonance of Layer-by-layer Gold Nanoparticles Induced Photoelectric Current in Environmentally-friendly Plasmon-sensitized Solar Cell. *Light: Sci. Appl.* **2012**, *1*, e14.
(42) Xu, M. F.; Zhu, X. Z.; Shi, X. B.; Liang, J.; Jin, Y.; Wang, Z. K.; Liao, L. S. Plasmon Resonance Enhanced Optical Absorption in Inverted Polymer/Fullerene Solar Cells with Metal Nanoparticle-Doped Solution-Processable TiO_2 Layer. *ACS Appl. Mater. Interfaces* **2013**, *5*, 2935−2942.
(43) Derkacs, D.; Lim, S. H.; Matheu, P.; Mar, W.; Yu, E. T. Improved Performance of Amorphous Silicon Solar Cells via Scattering from Surface Plasmon Polaritons in Nearby Metallic Nanoparticles. *Appl. Phys. Lett.* **2006**, *89*, 093103−093105.
(44) Konda, R. .; Mundle, R.; Mustafa, H.; Bamiduro, O.; Pradhan, A. .; Roy, U. .; Cui, Y.; Burger, A. Surface Plasmon Excitation via Au Nanoparticles in n-CdSe/p-Si Heterojunction Diodes. *Appl. Phys. Lett.* **2007**, *91*, 191111.
(45) Kim, K.; Carroll, D. L. Roles of Au and Ag Nanoparticles in Efficiency Enhancement of Poly(3-octylthiophene)/C_{60} Bulk Heterojunction Photovoltaic Devices. *Appl. Phys. Lett.* **2005**, *87*, 203113.
(46) Gole, A.; Murphy, C. J. Polyelectrolyte-Coated Gold Nanorods: Synthesis, Characterization and Immobilization. *Chem. Mater.* **2005**, *17*, 1325−1330.
(47) Garcia-Belmonte, G.; Boix, P. P.; Bisquert, J.; Sessolo, M.; Bolink, H. J. Simultaneous Determination of Carrier Lifetime and Electron Density-of-states in P3HT:PCBM Organic Solar Cells under Illumination by Impedance Spectroscopy. *Sol. Energy Mater. Sol. Cells* **2010**, *94*, 366−375.
(48) Fabregat-Santiago, F.; Garcia-Belmonte, G.; Mora-Seró, I.; Bisquert, J. Characterization of Nanostructured Hybrid and Organic Solar Cells by Impedance Spectroscopy. *Phys. Chem. Chem. Phys.* **2011**, *13*, 9083−9118.
(49) Liao, H. C.; Tsao, C. S.; Lin, T. H.; Jao, M. H.; Chuang, C. M.; Chang, S. Y.; Huang, Y. C.; Shao, Y. T.; Chen, C. Y.; Su, C. J.; Jeng, U. S.; Chen, Y. F.; Su, W. F. Nanoparticle-Tuned Self-Organization of a Bulk Heterojunction Hybrid Solar Cell with Enhanced Performance. *ACS Nano* **2012**, *6*, 1657−1666.

DOI: 10.1021/acsami.5b03024
ACS Appl. Mater. Interfaces 2015, 7, 15848−15854